

# Error estimate of the Non-Intrusive Reduced Basis (NIRB) two-grid method with parabolic equations

September 16, 2022

Elise Grosjean <sup>1</sup>, Yvon Maday <sup>2 3</sup>

## Abstract

Reduced Basis Methods (RBMs) are often proposed to approximate solutions of parametric problems. They are useful both to compute solutions for a large number of parameter values (e.g. for parameter fitting) and to approximate a solution for a new parameter value (e.g. real time approximation with a very high accuracy). They aim at reducing the computational costs of High Fidelity (HF) codes. They require well chosen solutions, called snapshots, preliminary computed (e.g. offline) with a HF classical method, involving, e.g. a fine mesh (finite element or finite volume) and generally require a profound modification of the HF code, in order for the online computation to be performed in short (or even real) time.

In this paper, we will focus on the Non-Intrusive Reduced Basis (NIRB) two-grid method. Its main advantage is its efficient way of using the HF code exclusively as a “black-box”, unlike other so-called intrusive methods which require a modification of the code. This is very convenient when the HF code is a commercial one and has been purchased, as is often the case in the industry. The effectiveness of this method relies on its decomposition into two stages, one offline (classical in most RBMs as presented above) and one online. The offline part is time-consuming but it is executed only once. On the contrary, the specificity of the NIRB approach is to solve, during the online part, the parametric problem on a coarse mesh only, and then to improve its precision. It is thus much cheaper than a HF evaluation. This method has been initially developed in the context of elliptic equations with finite element and has been extended to finite volume.

In this paper, we generalize the NIRB two-grid method to parabolic equations. To the best of our knowledge, the two-grid method has not already been studied in the context of time-dependent problems. With a model problem, which is the heat equation, we recover optimal estimates in  $L^\infty(0, T; H^1(\Omega))$ , and present numerical results.

## 1 Introduction

(RB<sup>n</sup>)

only requir

to implement

Let  $\Omega$  be a bounded domain in  $\mathbb{R}^d$ , with  $d \leq 3$  with smooth enough boundary  $\partial\Omega$ , and let us consider a parametric problem  $\mathcal{P}$  on  $\Omega$ . Non-Intrusive Reduced Basis (NIRB) methods are an alternative to classical reduced basis methods to approximate the solutions of such problems where the parameter is denoted as  $\mu$ , in a given set  $\mathcal{G}$  [8, 9] (see also different NIRB methods [5, 1] from the two-grid method). They may be more practical than intrusive RBMs from an engineering point of view since their uses are simplified by the execution of the HF code only as a “black-box” solver. These methods rely on the assumption that the manifold of all solutions  $\mathcal{S} = \{u(\mu), \mu \in \mathcal{G}\}$  has a small Kolmogorov width [18].

Like non RB<sup>n</sup> ; NIRB

high fidelity

## 10 Reminders on the NIRB two-grid method for stationary problems

The two-grid method, in the context of a HF solver of finite element or finite volume type, involves two partitioned meshes (or “grid”), one fine mesh  $\mathcal{M}_h$  and one coarse  $\mathcal{M}_H$ , where the respective sizes  $h$  and  $H$  of the meshes are such that  $h \ll H$ . The size  $h$  (respectively  $H$ ) is defined as

$$h = \max_{K \in \mathcal{M}_h} h_K \text{ (respectively } H = \max_{K \in \mathcal{M}_H} H_K\text{)}, \quad (1)$$

<sup>1</sup>Felix-Klein-Institut für Mathematik, Kaiserslautern TU, 67657, Deutschland

<sup>2</sup>Sorbonne Université and Université de Paris Cité, CNRS, Laboratoire Jacques-Louis Lions (LJLL), F-75005 Paris, France

<sup>3</sup>Institut Universitaire de France

where the diameter  $h_K$  (or  $H_K$ ) of any element  $K$  in a mesh is equal to  $\sup_{x,y \in K} |x - y|, K \in M_h$  (or  $\in M_H$ ).

*6ns blocks*

The fine mesh is used for the generation of the Reduced Basis (RB), and the coarse one is used to roughly and rapidly approximate the solution. This coarse mesh and the offline-online decomposition of the algorithm are <sup>15</sup> the key ingredients to the reduction of the complexity. Thus, using the notations for elliptic equations, we carry out the following decomposition:

*an alternation is to un?*

- First, the RB functions which belong to the reduced space denoted  $X_h^N$  are prepared in an "offline" stage with the fine mesh through a greedy procedure [4] or a Proper Orthogonal Decomposition (POD) [22, 2, 16]. The greedy procedure is a way to compute the modes by choosing iteratively some suitable parameters  $\mu_1, \dots, \mu_N \in \mathcal{G}$  and computes the approximate solutions  $u_h(\mu_1), \dots, u_h(\mu_N)$ . This part is costly in time, but only executed once, as for other RBMs. At the end of this stage, we obtain  $N L^2$ -orthonormalized basis functions, denoted  $(\Phi_i^h)_{i=1,\dots,N}$ . ~~At the end of this stage, we obtain  $N L^2$ -orthonormalized basis functions, denoted  $(\Psi_i^h)_{i=1,\dots,N}$~~  after processing a Gram-Schmidt orthonormalization algorithm. In order to enhance the results we may further perform the following eigenvalue problem:

$$\begin{cases} \text{Find } \Phi^h \in X_h^N \text{ and } \lambda \in \mathbb{R} \text{ such that:} \\ \forall v \in X_h^N, \int_{\Omega} \nabla \Phi^h \cdot \nabla v \, d\mathbf{x} = \lambda \int_{\Omega} \Phi^h \cdot v \, d\mathbf{x}, \end{cases} \quad (2)$$

*Xe pas d'fini*

and we get an increasing sequence of eigenvalues  $\lambda_i$ , and orthogonal eigenfunctions  $(\Phi_i^h)_{i=1,\dots,N}$ , orthonormalized in  $L^2(\Omega)$  and thus orthogonal in  $H^1(\Omega)$ , and define a new basis of the space  $X_h^N$ .

- Then, for a new parameter  $\mu$  for which we are interested in estimating the solution, a coarse approximation  $u_H(\mu)$  of the solution is first computed "online". This coarse approximation is of course not of sufficient precision but it is calculated much more rapidly compared to the fine mesh one. The NIRB post-processing then makes it possible to notably improve the precision by projection on the RB, within a very short runtime [8, 6, 12, 9]. The classical NIRB approximation is given by *Projecting  $u_H(\mu)$*

$$u_{Hh}^N(\mu) := \sum_{i=1}^N (u_H(\mu), \Phi_i^h) \Phi_i^h.$$

*which leads to*

As proposed in [7], we may also introduce a rectification matrix, denoted  $\mathbf{R}$ , computed from the coarse snapshots. ~~The~~ l letters are generated with the same parameters as for the fine snapshots (during the offline part). Then, we compute the vectors

$$\mathbf{R}_i = (\mathbf{A}^T \mathbf{A} + \delta \mathbf{I}_N)^{-1} \mathbf{A}^T \mathbf{B}_i, \quad i = 1, \dots, N, \quad (3)$$

where

$$u_{Hh}^N(\mu) \approx \sum_i R_i \Phi_i^h, \quad i = 1, \dots, N,$$

*We remark that  $u_{Hh}^N(\mu)$  is not yet  $u_H(\mu)$ , this is why we need this and*

$$u_{Hh}^N(\mu) = \sum_i R_i \Phi_i^h = \sum_i (u_H(\mu), \Phi_i^h) \Phi_i^h, \quad (4)$$

$$B_{k,i} = \int_{\Omega} \mathbf{u}_h(\mu_k) \cdot \Phi_i^h \, d\mathbf{x}, \quad (5)$$

$\mathbf{I}_N$  refers to the identity matrix and  $\delta$  is a regularization term [8]. The post-treatment applied to NIRB approximation reads

$$Ru_{Hh}^N(\mu) := \sum_{i,j=1}^N R_{ij} (u_H(\mu), \Phi_j^h) \Phi_i^h,$$

*when  $R_{ii} = 1$*

where  $(\cdot, \cdot)$  denotes the  $L^2$ -inner product. Note that, up to the relaxation parameter  $\delta$  the rectification process allows to retrieve the fine coefficients (given in (5)) from the coarse ones (given in (4)) for the parameters  $\mu = \mu_k, k = 1, \dots, N$ .

$$u_{Hh}^N(\mu_k) = u_H(\mu_k)$$

\*1, \*2 11-12] sont au niveau, mais n'as pas la même forme, mais des sous sections appealing for

\*2

**Motivation and earlier works.** The two-grid method, which can be used for several types of PDEs and approximations, is easy to implement. Moreover, its non-intrusive nature makes it applicable to a wide range of problems. Yet, to the best of our knowledge, this method has not already been studied nor implemented in the context of time-dependent problems [6, 8, 9, 23]. The two-grid method has been developed and analyzed in the context of  $P_1$  FEM (with Céa's and Aubin-Nitsche's lemmas) in [7] for second order elliptic equations. The energy-error estimate then is given by

$$\|u(\mu) - u_{Hh}^N(\mu)\|_{H^1(\Omega)} \leq \varepsilon(N) + C_1 h + C_2(N) H^2, \quad (6)$$

where  $C_1$  and  $C_2$  are constants independent of  $h$  and  $H$ ,  $C_2$  depends on  $N$ . The term  $\varepsilon(N)$  depends on a proper choice of the reduced basis space as a surrogate for the best approximation space associated to the Kolmogorov  $N$ -width. It decreases when  $N$  increases and it is linked to the error between the fine solution and its projection on  $X_h^N$ , given by

$$\left\| u_h(\mu) - \sum_{i=1}^N (u_h(\mu), \Phi_i^h) \Phi_i^h \right\|_{H^1(\Omega)}. \quad (7)$$

The second term in (6),  $C_1 h$ , is a contribution obtained through Céa's lemma for the reduced basis elements and the second one,  $C_2(N) H^2$ , through Aubin-Nitsche's lemma for the coarse grid approximation of  $u(\mu)$ . A trade-off needs to be done between increasing  $N$  to obtain a more accurate manifold, and keeping a constant  $C_2$  as low as possible.

This two-grid method has also been generalized and analyzed in the context of finite volume schemes [12] where a surrogate to Aubin-Nitsche's is used.

This article is about extending NIRB to time-dependent problems and performing its numerical analysis, in the setting of parabolic equations.

\*3

## Outline of the paper.

car

We will first theoretically prove that we recover optimal estimates in  $L^\infty(0, T; H^1(\Omega))$ , and then present numerical results 5. Our main result is given by the theorem 4.1 on the numerical analysis of convergence of the approach. The rest of this paper is organized as follows. In section 2 we describe the mathematical context. In section 3 we present the two-grids method in the context of parabolic equations. Section 4 is devoted to the proof of theorem 4.1. In the last section 5, the implementation is discussed and we illustrate the theoretical results with numerical results on the NIRB method with rectification.

2

## Mathematical Background

### 2.1 The continuous problem

In the next sections,  $C$  will denote various positive constants independent of the size of the meshes  $h$  and  $H$  and of the parameter  $\mu$ , and  $C(\mu)$  will denote constants independent of the size of the meshes  $h$  and  $H$  but dependent of  $\mu$ . We will consider the following heat equation on the domain  $\Omega$  and with homogeneous Dirichlet conditions, which takes the form

Like in

$$u_t - \mu \Delta u = f, \text{ in } \Omega \times ]0, T],$$

$$u(\mathbf{x}, 0) = u_0(\mathbf{x}), \text{ in } \Omega,$$

$$u(\mathbf{x}, t) = 0, \text{ on } \partial\Omega \times ]0, T],$$

(., t)

of  $u$  with up to him  
with respect to time

(8)

where  $f \in L^2(\Omega \times [0, T])$ , for any  $t > 0$ ,  $u(\cdot, t) \in H_0^1(\Omega)$ ,  $u_t \in L^2(\Omega)$  stands for the derivative,  $u_0 \in H_0^1(\Omega)$  and  $0 < \mu \in \mathcal{G}$  is the parameter. In analogy with the previous work on the NIRB FEM applied to elliptic equations, we consider one fine spatial grid for computing "offline" the snapshots associated with few values of the parameter and one coarse grid for the coarse solution, with sizes respectively denoted as  $h$  for the fine mesh and  $H$  for the coarse mesh (with  $h \ll H$ ). These grids are used for the spacial discretizations of the weak formulation of problem (8). A time stepping method is used to get a fully discrete approximation of the solution of (8). On our model problem we employed  $P_1$  finite elements for the discretization in space. For the time discretization, we considered finite difference approximation of the time derivative.

We consider two time grids, ending with at time  $T$ .

\*4 est remonté ici

of finite difference type

- One time grid, denoted  $F$ , is employed for the fine solution (for the snapshots construction). To avoid making notations more cumbersome, we will consider a uniform time grid with  ~~$\Delta t_F$  the interval between two time values~~. The time levels can be written  $t^n = n \Delta t_F$ , where  $n \in \mathbb{N}^*$ .
- Another time grid, denoted  $G$ , is used for the coarse solution. By analogy with the fine grid, we consider a uniform grid with time step  $\Delta t_G$ . Now, the time levels are written  $\tilde{t}^m = m \Delta t_G$ , where  $m \in \mathbb{N}^*$ .

55

The NIRB algorithm allows us to recover the optimal estimate in space, as in the previous analysis with elliptic equations. There is no such argument as the Aubin-Nitsche's one for time stepping method, hence we need to consider time discretizations that provide the same precision with different time steps hence we consider a higher order time scheme for the coarse solution.

60

Thus, we deal with ~~three~~ <sup>2</sup> kind of notations:

~~levels~~

~~dyne dt + Part~~

- $u(\mathbf{x}, t)$  denotes the true solution at time  $t \geq 0$  for  $\mathbf{x} \in \Omega$ .
- $u_h(\mathbf{x}, t)$  and  $u_H(\mathbf{x}, t)$  that respectively denote the fine and coarse solutions of the spatially semidiscrete solution, at time  $t \geq 0$ .
- $u_h^n(\mathbf{x})$  and  $u_H^m(\mathbf{x})$  that respectively denote the fine and coarse full-discretized solutions at time  $t^n = n \times \Delta t_F$  and  $\tilde{t}^m = m \times \Delta t_G$ , where  ~~$\Delta t_F$  is the fine time step, and  $\Delta t_G$  is the coarse one~~.

**Remark 2.1.** To simplify the notations, we consider that both time simulations end at time  $T$ .

hence  $T = N_F \Delta t_F$

$= M_G \Delta t_G$

We use the conventional notations for space-time dependent Sobolev spaces

In what follows

$$L^p(0, T; V) := \{u(\mathbf{x}, t) \mid \|u\|_{L^p(0, T; V)} := \left( \int_0^T \|u(\cdot, t)\|_V^p dt \right)^{1/p} < \infty\}, \quad 1 \leq p < \infty,$$

$$L^\infty(0, T; V) := \{u(\mathbf{x}, t) \mid \|u\|_{L^\infty(0, T; V)} := \text{ess sup}_{0 \leq t \leq T} \|u(\cdot, t)\|_V < \infty\},$$

where  $V$  is a real Banach space with norm  $\|\cdot\|_V$ . The variational form of (8) is given by:

$$\left\{ \begin{array}{l} \text{Find } u \in L^2(0, T; H_0^1(\Omega)) \text{ with } u_t \in L^2(0, T; H^{-1}(\Omega)) \text{ such that} \\ (u_t, v) + a(u, v; \mu) = (f, v), \quad \forall v \in H_0^1(\Omega) \text{ and } t \in (0, T), \\ u(\cdot, 0) = u_0, \text{ in } \Omega, \end{array} \right. \quad (9)$$

where  $a$  is given by

$$a(w, v; \mu) = \int_{\Omega} \mu \nabla w(\mathbf{x}) \cdot \nabla v(\mathbf{x}) d\mathbf{x}, \quad \forall w, v \in H_0^1(\Omega). \quad (10)$$

We remind that (9) is well posed (see [10] for the existence and the uniqueness of solutions to problem (9)) and we refer to the notations of [10].

**Remark 2.2.** (On the stability). We intend to state estimates for the NIRB approximation for all time snapshots  $n$ , that is related to maximum-norm in time with the either  $L^2$  norm or  $H^1$  norm in space, ie in  $L^\infty(0, T; L^2(\Omega))$  and  $L^\infty(0, T; H^1(\Omega))$ , which is stronger than with the usual stability study of the parabolic equation (8). Let us remind the classical (or less standard) stability results. We derive from (9) by using  $v = u$

$$(u_t, u) + \mu \|\nabla u\|^2 = |(f, u)|. \quad (11)$$

From the Young and Poincaré inequalities, there exists  $C > 0$  such that

$$|(f, u)| \leq \left( \frac{1}{2\mu} \|f\|^2 \right) + \frac{\mu}{2} \|\nabla u\|^2.$$

and since

$$(u_t, u) = \frac{1}{2} \frac{d}{dt} \|u\|^2,$$

(11) yields

$$\frac{d}{dt} \|u\|^2 + \mu \|\nabla u\|^2 \leq \frac{1}{\mu} \|f\|^2,$$

and integrating over  $(0, t)$  for all  $t \leq T$ , we end up with

$$\|u(t)\|^2 + \mu \int_0^t \|\nabla u(s)\|^2 ds \leq C(\|u_0\|^2 + \frac{1}{\mu} \int_0^t \|f(s)\|^2 ds),$$

which gives

$$\|u\|_{L^\infty(0,T;L^2(\Omega))}^2 + \mu \|u\|_{L^2(0,T;H_0^1(\Omega))}^2 \leq C(\|u_0\|_{L^2(\Omega)}^2 + \frac{1}{\mu} \|f\|_{L^2(0,T;L^2(\Omega))}^2).$$

That establishes the first stability result.

For the  $L^\infty$  stability in time and  $H^1$  in space, we proceed the same with  $v = u_t$  in (9). Integrating over  $(0, t)$  for all  $t \leq T$ , it yields

$$\int_0^t \|u_t(s)\|^2 ds + \mu \int_0^t \frac{d}{dt} \|\nabla u(s)\|^2 ds \leq \int_0^t \|f(s)\|^2 ds,$$

which gives

$$\int_0^t \|u_t(s)\|^2 ds + \mu \|\nabla u(t)\|^2 \leq \mu \|\nabla u_0\|^2 + \int_0^t \|f(s)\|^2 ds,$$

and we obtain

$$\|u\|_{L^\infty(0,T;H_0^1(\Omega))}^2 \leq \|\nabla u_0\|_{L^2(\Omega)}^2 + \frac{1}{\mu} \|f\|_{L^2(0,T;L^2(\Omega))}^2.$$

2.2 The various discretizations

Let  $V_h$  and  $V_H$  consists of continuous piecewise linear finite element functions which vanish on the boundary  $\partial\Omega$ . We consider the projection operator  $P_h^1$  on  $V_h$  ( $P_H^1$  on  $V_H$  is defined similarly) which is given by

$$(\nabla P_h^1 u, \nabla v) = (\nabla u, \nabla v), \quad \forall v \in V_h, \quad (12)$$

The semi-discrete form of the variational problem (9) writes for the fine mesh (similarly for the coarse mesh):

$$\left\{ \begin{array}{l} \text{Find } u_h(t) = u_h(\cdot, t) \in V_h \text{ for } t \geq 0 \text{ such that} \\ (\partial_t u_h, v_h) + a(u_h, v_h; \mu) = (f(t), v_h), \quad \forall v_h \in V_h \text{ and } n \geq 1, \\ u_h(\cdot, 0) = u_h^0 = P_h^1(u^0), \end{array} \right. \quad (13)$$

The full discrete form of the variational problem (9) for the fine mesh with implicit Euler scheme writes:

$$\left\{ \begin{array}{l} \text{Find } u_h^n \in V_h \text{ for } n \geq 0 \text{ such that} \\ (\bar{\partial} u_h^n, v_h) + a(u_h^n, v_h; \mu) = (f(t^n), v_h), \quad \forall v_h \in V_h \text{ and } n \geq 1, \\ u_h(\cdot, 0) = u_h^0, \end{array} \right. \quad (14)$$

where the time derivative in the variational form of the problem (13) has been replaced by a backward difference quotient,  $\bar{\partial} u_h^n = \frac{u_h^n - u_h^{n-1}}{\Delta t_F}$ ,

and with Crank-Nicholson scheme, and  $\bar{\partial} u_H^m = \frac{u_H^m - u_H^{m-1}}{\Delta t_G}$ , it becomes, for the coarse mesh:

$$\left\{ \begin{array}{l} \text{Find } u_H^m \in V_H \text{ for } m \geq 0, \text{ such that} \\ (\bar{\partial} u_H^m, v_H) + a(\frac{u_H^m + u_H^{m-1}}{2}, v_H; \mu) = (f(\tilde{t}^{m-\frac{1}{2}}), v_H), \quad \forall v_H \in V_H \text{ and } m \geq 1, \\ u_H(\cdot, 0) = u_H^0, \end{array} \right. \quad (15)$$

where  $\tilde{t}^{m-\frac{1}{2}} = \frac{\tilde{t}^m + \tilde{t}^{m-1}}{2}$ . Let  $\tilde{u}_H^n$  be the quadratic interpolation in time of the coarse solution at time  $t^n \in I_m = [\tilde{t}^{m-1}, \tilde{t}^m]$  defined on  $[\tilde{t}^{m-2}, \tilde{t}^m]$  from the values  $u_H^{m-2}, u_H^{m-1}$ , and  $u_H^m$ , for all  $m = 2, \dots, \frac{T}{\Delta t_G}$ . We choose this interpolation in order to keep an approximation of order 2 in time  $\Delta t_G$  (it works also with other quadratic interpolations). We will consider the solutions of (14), and we seek the NIKB approximation with the form

$$u_{Hh}^{N,n}(x; \mu) = \sum_{i=1}^N \alpha_i^H(\mu, t^n) \Phi_i^h(x), \quad n \geq 0, \quad (16)$$

where  $\alpha_i^H$  are the coarse coefficients and are defined by

$$\alpha_i^H(\mu, t^n) = (\tilde{u}_H^p(\mu), \Phi_i^h), \quad (17)$$

where  $(\Phi_i^h)_{i=1,\dots,N}$  denotes the  $L^2$  and  $H^1$  orthonormalized basis functions obtained through a greedy procedure (see algorithms 2 or 1 below). Note that they do not depend on time, only the coefficients are time-dependent. This strategy will be detailed in section 3.

~~Before entering in the proof details of Theorem 4.1, we require a few theorems from [24], on the FEM classical estimates and on both finite difference schemes employed. In the following theorems, we require that the solution of the continuous problem has the regularity implicitly assumed by the presence of the norms on the right. It is well known that with a FEM semi-discretization in space, the following estimates hold:~~

**Theorem 2.3** (Theorem 1.2 [24]). Let  $\Omega$  be a convex polyhedron. Let  $u \in W^{1,1}(0, T; H^2(\Omega))$  be the solution of (8) with  $u_0 \in H^2(\Omega)$  and  $u_h$  be the semidiscretized variational form (13). Assume that  $u_0 = 0$  on  $\partial\Omega$ , then

$$\text{for } t \geq 0, \quad \|u(t) - u_h(t)\|_{L^2(\Omega)} \leq C(\mu)h^2 \left[ \|u_0\|_{H^2(\Omega)} + \int_0^t \|u_t\|_{H^2(\Omega)} ds \right], \quad (18)$$

Once fully discretized on a fine mesh with the backward Euler Galerkin method, the estimate (18) is replaced by the following estimate.

**Theorem 2.4** (Theorem 1.5 [24]). Let  $\Omega$  be a convex polyhedron and. With  $u_h^n$  and  $u$  be the solutions of (14) and (8), respectively. If  $\|u_h^0 - u_0\| \leq Ch^2 \|u_0\|_{H^2(\Omega)}$ , and  $u_0 = 0$  on  $\partial\Omega$ , we have

$$\forall n \geq 0, \quad \|u(t^n) - u_h^n\|_{L^2(\Omega)} \leq C(\mu)h^2 \left[ \|u_0\|_{H^2(\Omega)} + \int_0^{t^n} \|u_t\|_{H^2(\Omega)} ds \right] + \Delta t_F \int_0^{t^n} \|u_{tt}\|_{L^2(\Omega)} ds, \quad (19)$$

**Theorem 2.5** (Theorem 1.4 [24]). Let  $\Omega$  be a convex polyhedron. Let  $u \in H^1(0, T; H^2(\Omega)) \cap L^2(0, T; H^2(\Omega))$  be the solution of (8) with  $u_0 \in H^2(\Omega)$  and  $u_h$  be the semidiscretized variational form (13), we have

$$\text{for } t \geq 0, \quad \|\nabla u(t) - \nabla u_h(t)\|_{L^2(\Omega)} \leq C(\mu)h \left[ \|u_0\|_{H^2(\Omega)} + \|u(t)\|_{H^2(\Omega)} + \left( \int_0^t \|u_t\|_{H^1(\Omega)}^2 ds \right)^{1/2} \right], \quad (20)$$

~~where  $C$  depends on the parameter  $\mu$ .~~

The estimate (20) with the full discretization leads to the following theorem.

**Theorem 2.6.** Let  $\Omega$  be a convex polyhedron. Let  $u \in H^1(0, T; H^2(\Omega)) \cap H^2(0, T; L^2(\Omega))$  be the solution of (8) with  $u_0 \in H^2(\Omega)$  and  $u_h$  be the semidiscretized variational form (13), we have

$$\forall n \geq 0, \quad \|\nabla u_h^n - \nabla u(t^n)\|_{L^2(\Omega)} \leq C(\mu)h \left[ \|u_0\|_{H^2(\Omega)} + \left( \int_0^{t^n} \|u_t\|_{H^2(\Omega)}^2 ds \right)^{1/2} \right]$$

*I may use some constants in +  $\Delta t_F \left( \int_0^{t^n} \|\nabla u_{tt}\|_{L^2(\Omega)}^2 ds \right)^{1/2}$ .*

$$(21)$$

*Proof.* This may be proven by following the same lines as in the proof on the  $L^2$  estimate (Theorem 1.5 [24]), as it is highlighted in [24]. We first decompose the error with two components  $e^n$  and  $\rho^n$  such that

$$\begin{aligned} \forall n \geq 1, \quad e^n &:= \sqrt{\mu}(\nabla u_h^n - \nabla u(t^n)) = \sqrt{\mu}((\nabla u_h^n - \nabla P_h^1 u(t^n)) + (\nabla P_h^1 u(t^n) - \nabla u(t^n))) \\ &= \sqrt{\mu}(\nabla \theta^n + \nabla \rho^n). \end{aligned} \quad (22)$$

- For the estimate on  $\rho$ , a classical FEM estimate [24, 3] is

$$\|P_h^1 v - v\|_{L^2(\Omega)} + h \|\nabla(P_h^1 v - v)\|_{L^2(\Omega)} \leq Ch^2 \|v\|_{H^2(\Omega)}, \quad v \in H^2 \cap H_0^1,$$

which leads to

$$\|\nabla \rho^n\| \leq Ch \|u(t^n)\|_{H^2(\Omega)}, \quad \forall n \geq 0,$$

and it leads to ,

$$\|\nabla \rho^n\| \leq Ch \left[ \|u_0\|_{H^2(\Omega)} + \int_0^{t^n} \|u_t\|_{H^2(\Omega)} ds \right]. \quad (23)$$

- For the estimate on  $\theta$ , let us consider  $v \in V_h$ . Since the operators  $P_h^1$  and  $\bar{\partial}$  commute, we write

$$(\bar{\partial}\theta^n, v) + \mu(\nabla\theta^n, \nabla v) = (\bar{\partial}u_h^n, v) - (P_h^1\bar{\partial}u(t^n), v) + \mu(\nabla u_h^n, \nabla v) - \mu(\nabla P_h^1u(t^n), \nabla v).$$

From (9) and (14), it implies

$$\begin{aligned} (\bar{\partial}\theta^n, v) + \mu(\nabla\theta^n, \nabla v) &= (f, v) - (P_h^1\bar{\partial}u(t^n), v) - \mu(\nabla P_h^1u(t^n), \nabla v), \\ &= (f, v) - (P_h^1\bar{\partial}u(t^n), v) - \mu(\nabla u(t^n), \nabla v), \text{ by definition of } P_h^1, \\ &= (u_t(t^n), v) - (P_h^1\bar{\partial}u(t^n), v). \end{aligned}$$

Then, with a triangle inequality, it yields

$$\begin{aligned} (\bar{\partial}\theta^n, v) + \mu(\nabla\theta^n, \nabla v) &= -((P_h^1 - I)\bar{\partial}u(t^n), v) - ((\bar{\partial}u(t^n) - u_t(t^n)), v) \\ &:= -(w_1^n + w_2^n, v) = -(w^n, v). \end{aligned} \tag{24}$$

Instead of replacing  $v$  by  $\theta^n$  as in the  $L^2$  estimate, here we replace  $v$  by  $\bar{\partial}\theta^n$ , thus the equation (24) takes the form

$$(\bar{\partial}\theta^n, \bar{\partial}\theta^n) + \mu(\nabla\theta^n, \bar{\partial}\nabla\theta^n) = -(w^n, \bar{\partial}\theta^n).$$

Therefore, by definition of  $\bar{\partial}$  for the Backward Euler discretization,

$$\underbrace{(\bar{\partial}\theta^n, \bar{\partial}\theta^n) + \mu \frac{\|\nabla\theta^n\|_{L^2(\Omega)}^2}{\Delta t_F} - \mu \frac{(\nabla\theta^n, \nabla\theta^{n-1})}{\Delta t_F}}_{T_a} = -(w^n, \bar{\partial}\theta^n).$$

With Young's inequality,

$$(\nabla\theta^n, \nabla\theta^{n-1}) \leq \frac{1}{2}\|\nabla\theta^n\|_{L^2(\Omega)}^2 + \frac{1}{2}\|\nabla\theta^{n-1}\|_{L^2(\Omega)}^2.$$

Thus,

$$\|\bar{\partial}\theta^n\|_{L^2(\Omega)}^2 + \mu \frac{\|\nabla\theta^n\|_{L^2(\Omega)}^2}{2\Delta t_F} - \mu \frac{\|\nabla\theta^{n-1}\|_{L^2(\Omega)}^2}{2\Delta t_F} \leq T_a \leq \frac{1}{2}\|w^n\|_{L^2(\Omega)}^2 + \frac{1}{2}\|\bar{\partial}\theta^n\|_{L^2(\Omega)}^2,$$

and it results in

$$\|\bar{\partial}\theta^n\|_{L^2(\Omega)}^2 + \mu \frac{\|\nabla\theta^n\|_{L^2(\Omega)}^2}{\Delta t_F} \leq \mu \frac{\|\nabla\theta^{n-1}\|_{L^2(\Omega)}^2}{\Delta t_F} + \|w^n\|_{L^2(\Omega)}^2.$$

Since  $\|\bar{\partial}\theta^n\|_{L^2(\Omega)}^2 \geq 0$ , it follows that

$$\forall n \geq 1, \|\nabla\theta^n\|_{L^2(\Omega)}^2 \leq \|\nabla\theta^{n-1}\|_{L^2(\Omega)}^2 + \frac{\Delta t_F}{\mu} \|w^n\|_{L^2(\Omega)}^2,$$

and we recursively obtain

$$\forall n \geq 1, \|\nabla\theta^n\|_{L^2(\Omega)}^2 \leq \|\nabla\theta^0\|_{L^2(\Omega)}^2 + \frac{\Delta t_F}{\mu} \sum_{j=1}^n \|w^j\|_{L^2(\Omega)}^2.$$

By definition of  $\theta$  (and  $P_h^1$ ),

$$\begin{aligned} \|\nabla\theta^0\|_{L^2(\Omega)} &= \|\nabla u_h^0 - \nabla P_h^1u(t^0)\|_{L^2(\Omega)} \leq \|\nabla u_h^0 - \nabla u(t^0)\|_{L^2(\Omega)} + \|\nabla u(t^0) - \nabla P_h^1u(t^0)\|_{L^2(\Omega)} \\ &\leq \|\nabla u_h^0 - \nabla u(t^0)\|_{L^2(\Omega)} + Ch\|u(t^0)\|_{H^2(\Omega)}. \end{aligned}$$

It remains to estimate the  $L^2$  norm of the  $w^j$ , defined by (24).

$$\begin{aligned}
w_1^j &= (P_h^1 - I)\bar{\partial}u(t^j) \\
&= \frac{1}{\Delta t_F}(P_h^1 - I) \int_{t^{j-1}}^{t^j} u_t \, ds, \\
&= \frac{1}{\Delta t_F} \int_{t^{j-1}}^{t^j} (P_h^1 - I)u_t \, ds, \text{ since } P_h^1 \text{ and the time integral commute.}
\end{aligned}$$

Thus, from Hölder's inequality,

$$\begin{aligned}
\frac{\Delta t_F}{\mu} \sum_{j=1}^n \|w_1^j\|_{L^2(\Omega)}^2 &\leq \frac{\Delta t_F}{\mu} \sum_{j=1}^n \int_{\Omega} \left[ \frac{1}{\Delta t_F^2} \int_{t^{j-1}}^{t^j} ((P_h^1 - I)u_t)^2 \, ds \right] \Delta t_F \\
&\leq \frac{1}{\mu} \sum_{j=1}^n \int_{t^{j-1}}^{t^j} \|(P_h^1 - I)u_t\|_{L^2(\Omega)}^2 \, ds, \\
&\leq \frac{C}{\mu} h^4 \sum_{j=1}^n \int_{t^{j-1}}^{t^j} \|u_t\|_{H^2(\Omega)}^2 \, ds, \text{ by the definition of } P_h^1 \\
&\leq \frac{C}{\mu} h^4 \int_0^{t^n} \|u_t\|_{H^2(\Omega)}^2 \, ds. \tag{25}
\end{aligned}$$

- To estimate the  $L^2$  norm of the  $w_2$ , we write

$$\begin{aligned}
w_2^j &= \frac{1}{\Delta t_F}(u(t^j) - u(t^{j-1})) - u_t(t^j), \\
&= -\frac{1}{\Delta t_F} \int_{t^{j-1}}^{t^j} (s - t^{j-1}) u_{tt}(s) \, ds,
\end{aligned}$$

such that we end up with

$$\frac{\Delta t_F}{\mu} \sum_{j=1}^n \|w_2^j\|_{L^2(\Omega)}^2 \leq \frac{1}{\mu} \sum_{j=1}^n \left\| \int_{t^{j-1}}^{t^j} (s - t^{j-1}) u_{tt}(s) \, ds \right\|_{L^2(\Omega)}^2 \leq \frac{\Delta t_F^2}{\mu} \int_0^{t^n} \|u_{tt}\|_{L^2(\Omega)}^2 \, ds.$$

Combining the estimates on  $\rho$  and  $\theta$  concludes the proof. □

Finally, in the same manner, we can recover the estimate in  $H^2$  and  $\Delta t_G^2$  with the Crank-Nicolson scheme in the  $L^2$  norm

**Theorem 2.7** (Theorem 1.6 [24]). Let  $u_H^m$  be the solution given by (15), associated to Crank-Nicolson discretization with the coarse grids, and  $u$  be the solution of (8) belonging to  $H^2(0, T; H^2(\Omega)) \cap H^3(0, T; L^2(\Omega))$  such that  $u_0 \in H^2(\Omega)$ . Let  $\|u_0^H - u_0\| \leq CH^2 \|u_0\|_{H^2(\Omega)}$  ~~and  $u_{ttt}$  is bounded~~, then

$$\forall m \geq 0, \quad \|u(\tilde{t}^m) - u_H^m\|_{L^2(\Omega)} \leq CH^2 \left[ \|u_0\|_{H^2(\Omega)} + \int_0^{\tilde{t}^m} \|u_t\|_{H^2(\Omega)} \, ds \right] + C\Delta t_G^2 \left[ \left( \int_0^{\tilde{t}^m} \|u_{ttt}\|_{L^2(\Omega)}^2 \, ds \right)^{1/2} + \left( \int_0^{\tilde{t}^m} \|\Delta u_{tt}\|_{L^2(\Omega)}^2 \, ds \right)^{1/2} \right]$$

*via la méthode des deux mailles sur l'estimation déduite de Thm 2.7*

### 3 The Non-Intrusive Reduced Basis method (NIRB) in the context of parabolic equations

#### 3.1 Main steps

This section details the main steps of the two-grids method algorithm in the context of parabolic equations and more precisely how to employ a POD-Greedy algorithm [14, 13, 17] in order to define the reduced basis. Indeed,

in the time-discrete formulation, a single solution associated with a parameter  $\mu$  consists of a sequence of possibly several hundred snapshots over time (each snapshot being a high-fidelity finite element approximation in space at time  $t^n$ ). Hence, during the greedy algorithm, each greedy step is combined with a temporal compression step performed by a POD. Let us detail the different steps of our offline-online decomposition. The first three points are performed in the offline part, and the others are done online.

95

1. For each parameter  $(\mu_i)_{i \in \{1, \dots, N_{train}\}}$ , we compute fine snapshots  $\{\mathbf{u}_h^n(\mu_i)\}_{i \in \{1, \dots, N_{train}\}}$  with the ~~FETI~~ solver. We define  $\mathcal{G}_{train} = \bigcup_{i \in \{1, \dots, N_{train}\}} \mu_i$ . full discrete (14)
2. We generate the basis functions (time-independent)  $(\Phi_i^h)_{i=1, \dots, N}$  through a POD-Greedy algorithm as presented in algorithm 1. et toutes matriciennes

In the algorithms 2 and 1, the NIRB  $L^2$  fine projection at each step  $k$  is defined by

$$P^{k-1}(\mathbf{u}_h^n(\mu)) = \sum_{i=1}^{k-1} (\mathbf{u}_h^n(\mu), \Phi_i^h)_{L^2} \Phi_i^h. \quad (27)$$

*and the term* Remark

$$\|\mathbf{u}_h^n(\mu) - P^{k-1}(\mathbf{u}_h^n(\mu))\|_{L^2} \quad (28)$$

can be calculated either with a set of training snapshots or evaluated with an a-posteriori estimate. Since at each step  $k$ , all sets added in the basis are in the orthogonal complement of  $X_h^{k-1}$ , it yields an  $L^2$  orthogonal basis without further processing. In practice, the algorithm is halted with a stopping criterion such as an error threshold or a maximum number of basis functions to generate. Then, we solve the following eigenvalue problem:

$$\begin{cases} \text{Find } \Phi_h \in X_h^N, \text{ and } \lambda \in \mathbb{R} \text{ such that:} \\ \forall v \in X_h^N, \int_{\Omega} \nabla \Phi_h \cdot \nabla v \, d\mathbf{x} = \lambda \int_{\Omega} \Phi_h \cdot v \, d\mathbf{x}, \end{cases} \quad (29)$$

partir à la ligne

where  $X_h^N = \text{Span}\{\Phi_1^h, \dots, \Phi_N^h\}$ . We get an increasing sequence of eigenvalues  $\lambda_i$ , and orthogonal eigenfunctions  $(\Phi_i^h)_{i=1, \dots, N}$ , which do not depend on time, orthonormalized in  $L^2(\Omega)$  and orthogonalized in  $H^1(\Omega)$ . Note that with Gram-Schmidt procedure, we only obtain an  $L^2$ -orthonormalized RB.

105

3. For the rectification post-treatment, we generate the equivalent coarse snapshots and the rectification matrix with algorithm 3. telle chose ici
4. We solve the problem (8) on the coarse mesh  $T_H$  for a new parameter  $\mu \in \mathcal{G}$  at each time step  $m = 0, \dots, \frac{T}{\Delta t_H}$ . Let us denote by  $\widetilde{u}_H^m(\mu)$  the coarse solution at time  $\widetilde{t}^m$ . M, T

5. The coarse solutions are quadratically interpolated on the fine time grid, as for instance with the parabola defined on  $[\widetilde{t}^{m-2}, \widetilde{t}^m]$  with the values  $u_H^{m-2}, u_H^{m-1}, u_H^m$ :

For  $m \geq 2$ , for all  $n \in I_m = [\widetilde{t}^{m-1}, \widetilde{t}^m]$ ,

$$\begin{aligned} \widetilde{u}_H^n(\mu) &= \frac{u_H^{m-2}(\mu)}{(\widetilde{t}^m - \widetilde{t}^{m-2})(\widetilde{t}^{m-2} - \widetilde{t}^{m-1})} \left[ -(t^n)^2 + (\widetilde{t}^{m-1} + \widetilde{t}^m)t^n - t^{m-1}t^m \right] \\ &\quad + \frac{u_H^{m-1}(\mu)}{(\widetilde{t}^{m-2} - \widetilde{t}^{m-1})(\widetilde{t}^{m-1} - \widetilde{t}^m)} \left[ -(t^n)^2 + (\widetilde{t}^m + \widetilde{t}^{m-2})t^n - t^m t^{m-2} \right] \\ &\quad + \frac{u_H^m(\mu)}{(\widetilde{t}^{m-1} - \widetilde{t}^m)(\widetilde{t}^m - \widetilde{t}^{m-2})} \left[ -(t^n)^2 + (\widetilde{t}^{m-2} + \widetilde{t}^{m-1})t^n - t^{m-2}t^{m-1} \right]. \end{aligned} \quad (30)$$

For  $t^n \in I_1 = [\widetilde{t}^0, \widetilde{t}^1]$ , we use the parabola defined by the values  $u_H^0, u_H^1, u_H^2$

6. Then, we linearly interpolate  $\widetilde{u}_H^n(\mu)$  on the fine mesh in order to compute the  $L^2$ -inner product with the basis functions. The approximation used in the two-grid method is

$$\text{For } n = 0, \dots, \frac{T}{\Delta t_F}, u_{Hh}^{N,n}(\mu) := \sum_{i=1}^N (\widetilde{u}_H^n(\mu), \Phi_i^h) \Phi_i^h, \quad (31)$$

and with the rectification post-treatment step [8, 12], it becomes

$$R^{N,n}(\mu) := \sum_{i=1}^N R_{ij}^n (\tilde{u}_H^n(\mu), \Phi_j^h) \Phi_i^h, \quad (32)$$

where  $R^n$  is the rectification matrix at time  $t^n$  (see algorithm 3).

---

**Algorithm 1** POD-Greedy algorithm ~~with  $\mu_i \in \mathcal{G}_{train} \cap \{\mu_1, \dots, \mu_{N_{train}}\}$~~ 


---

**Input:**  $N_{max}$ ,  $\{\mathbf{u}_h^n(\mu_1), \dots, \mathbf{u}_h^n(\mu_{N_{train}})\}$  with  $\mu_i \in \mathcal{G}_{train} \cap \{\mu_1, \dots, \mu_{N_{train}}\}$   
**Output:** Reduced basis  $\{\Phi_1^h, \dots, \Phi_N^h\}$

Choose  $\mu_1 = \arg \max_{\mu \in \mathcal{G}_{train}} \|\mathbf{u}_h^n(\mu)\|_{L^\infty(0,T;L^2)}$ , then produce a family of  $L^2$ -orthonormalized modes  $\Phi_1, \dots, \Phi_{N_1} = POD(\{\mathbf{u}_h^n(\mu_1), n = 0, \dots, \frac{T}{\Delta t_F}\})$  (obtained with a small tolerance)  
Set  $\mathcal{G}_1 = \mu_1$  and  $X_h^1 = \text{span}\{\Phi_1, \dots, \Phi_{N_1}\}$ .  
**while**  $\sum_{k=1}^N N_k < N_{max}$  **do**  
     $\mu_k = \arg \max_{\mu \in \mathcal{G}_{train}} \frac{\|\mathbf{u}_h^n(\mu) - P^{k-1}(\mathbf{u}_h^n(\mu))\|_{L^\infty(0,T;L^2)}}{\|\mathbf{u}_h^n(\mu)\|_{L^\infty(0,T;L^2)}},$  with  $P^{k-1}$  defined by ~~27~~ non?  $\mu_k$  defines  $\mathcal{G}_k$   
     $\Phi_{N_{k-1}+1}, \dots, \Phi_{N_k} = POD(\{\mathbf{u}_h^n(\mu_k) - P^{k-1}(\mathbf{u}_h^n(\mu)), n = 0, \dots, \frac{T}{\Delta t_F}\})$   
    Set  $\mathcal{G}_k = \mathcal{G}_{k-1} \cup \mu_k$  and  $X_h^k = X_h^{k-1} \oplus \text{span}\{\Phi_{N_k+1}, \dots, \Phi_{N_k}\}$ .  
**end while**

! 110 **Remark 3.1.** A standard greedy algorithm may also be used but it increases the costs of the offline part. The time is considered as an additional parameter. In the following algorithm, a tolerance threshold is used instead of a priori given number of basis functions.

---

**Algorithm 2** Greedy algorithm

---

**Input:**  $N_{max}$ ,  $\{\mathbf{u}_h^n(\mu_1), \dots, \mathbf{u}_h^n(\mu_{N_{train}})\}$  with  $\mu_i \in \mathcal{G}_{train} \subset \mathcal{G}$ ,  $n = 0, \dots, \frac{T}{\Delta t_F}$   
**Output:** Reduced basis  $\{\Phi_1^h, \dots, \Phi_N^h\}$

Choose  $\mu_1, n_1 = \arg \max_{\mu \in \mathcal{G}_{train}, n \in \{0, \dots, \frac{T}{\Delta t_F}\}} \|\mathbf{u}_h^n(\mu)\|_{L^2(\Lambda)}$   
Set  $\Phi_1 = \frac{\mathbf{u}_h^{n_1}(\mu_1)}{\|\mathbf{u}_h^{n_1}(\mu_1)\|_{L^2}}$   
Set  $\mathcal{G}_1 = \mu_1, n_1$  and  $X_h^1 = \text{span}\{\Phi_1\}$ .  
**for**  $k = 2$  to  $N$  **do:**  
     $\mu_k, n_k = \arg \max_{\mu \in \mathcal{G}_{train}, n \in \{0, \dots, \frac{T}{\Delta t_F}\}} \|\mathbf{u}_h^n(\mu) - P^{k-1}(\mathbf{u}_h^n(\mu))\|_{L^2},$  with  $P^{k-1}$  defined by ~~27~~  
    Compute  $\widetilde{\Phi}_k = \mathbf{u}_h^{n_k}(\mu_k) - \sum_{i=1}^{k-1} (\mathbf{u}_h^n(\mu_k), \Phi_i)_{L^2} \Phi_i$  and set  $\Phi_k = \frac{\widetilde{\Phi}_k}{\|\widetilde{\Phi}_k\|_{L^2}}$   
    Set  $\mathcal{G}_k = \mathcal{G}_{k-1} \cup \mu_k$  and  $X_h^k = X_h^{k-1} \oplus \text{span}\{\Phi_k\}$   
    Stop when  $\|\mathbf{u}_h^n(\mu) - P^{k-1}(\mathbf{u}_h^n(\mu))\|_{L^2} \leq tol \forall \mu \in \mathcal{G}_{train}, \forall n = 0, \dots, \frac{T}{\Delta t_F}$ .  
**end for**

In the offline part, the rectification matrix is computed through the following algorithm

**Algorithm 3** algorithm for the offline rectification post-treatment

**Input:**  $\{\mathbf{u}_h^n(\mu_1), \dots, \mathbf{u}_h^n(\mu_{N_{train}})\}$ , with  $\mu_i \in \mathcal{G}_{train} \subset \mathcal{G}$ ,  $n = 0, \dots, \frac{T}{\Delta t_F}\}$  and with the same parameter  $\{\mathbf{u}_H^m(\mu_1), \dots, \mathbf{u}_H^m(\mu_{N_{train}})\}$ , with  $\mu_i \in \mathcal{G}_{train} \subset \mathcal{G}$ ,  $m = 0, \dots, \frac{T}{\Delta t_G}\}$

**Output:** Rectification matrix  $R_{ij}^n$ ,  $n = 0, \dots, \frac{T}{\Delta t_F}$

Realize the quadratic interpolation of the coarse snapshots in time, denoted  $\widetilde{\mathbf{u}}_H^n$ ,  $n = 0, \dots, \frac{T}{\Delta t_F}$  with (30).

for  $n = 0, \dots, \frac{T}{\Delta t_F}$ : do

Calculate the fine and coarse coefficients

$$\forall i = 1, \dots, N, \text{ and } \forall \mu_k \in \mathcal{G}_{train}, A_{k,i}^n = \int_{\Omega} \widetilde{\mathbf{u}}_H^n(\mu_k) \cdot \Phi_i^h d\mathbf{x}, \text{ and } B_{k,i}^n = \int_{\Omega} \mathbf{u}_h^n(\mu_k) \cdot \Phi_i^h d\mathbf{x},$$

$$\text{For } i = 1, \dots, N, \text{ set } R_i^n = (\mathbf{A}^n{}^T \mathbf{A}^n + \delta \mathbf{I}_N)^{-1} \mathbf{A}^n{}^T \mathbf{B}^n.$$

end for

In the subsequent section, we demonstrate the optimal error in  $L^\infty(0, T; H^1(\Omega))$ .

next

## 4 NIRB error estimate with parabolic equations

**Main result** Our main result is the following theorem.

**Theorem 4.1.** (NIRB error estimate for parabolic equations.) Let us consider the problem 8 and its exact solution  $u(\mathbf{x}, t; \mu)$ , and the full discretized solution to the problem 14. Let  $(\Phi_i^h)_{i=1, \dots, N}$  be the  $L^2$ -orthonormalized and  $H^1$ -orthogonalized RB generated with the POD-greedy algorithm 1 from the fine solutions of (14), on a fine mesh of size  $h$ , with  $\mathbb{P}_1$  FE for the spatial discretization, and a Backward Euler scheme for the time discretization. For  $m = 0, \dots, \frac{T}{\Delta t_G}$ , let  $\mathbf{u}_H^m(\mu)$  be the coarse approximation of (14) for  $\mu \in \mathcal{G}$ , on a coarse mesh of size  $H$ , with a  $\mathbb{P}_1$  FEM for the spatial discretization, and a Crank-Nicolson scheme for the time discretization.

120

Let us consider the NIRB approximation, defined by (16) and derived from these solutions. Then, the following estimate holds

$$\text{for } n = 0, \dots, \frac{T}{\Delta t_F}, \|u(t^n)(\mu) - u_{Hh}^{N,n}(\mu)\|_{H^1(\Omega)} \leq \varepsilon(N) + C_1(\mu)h + C_2(N)H^2 + C_3(\mu)\Delta t_F + C_4(N)\Delta t_G^2, \quad (33)$$

where  $C_1, C_2, C_3$  and  $C_4$  are constants independent of  $h$  and  $H$ ,  $\Delta t_F$  and  $\Delta t_G$ . The term  $\varepsilon$  depends on the Kolmogorov  $N$ -width and measures the error given by (7). If  $H$  is such as  $H^2 \sim h$ ,  $\Delta t_G^2 \sim \Delta t_F$ , and  $\varepsilon(N)$  is small enough, with  $C_2(N)$  and  $C_4(N)$  not too large, it results in an error estimate in  $\mathcal{O}(h + \Delta t_F)$ .

Theorem 4.1 proves that the NIRB two grids method can be applied to parabolic problems. We recover optimal error estimates in  $L^\infty(0, T; H^1(\Omega))$ . The NIRB two-grids method does not yield to optimal result in time, thus our choice of finite difference schemes is motivated by the fact that we want the coarse solution to be coarser in space as well as in time, compared to the fine solution.

**Remark 4.2.** This theorem can be generalized to  $\mathbb{P}_k$  FEM space, with  $k > 1$ .

With the  $L^2$  norm, we obtain the following theorem.

**Theorem 4.3.** With the same assumptions as in the theorem 4.1, with the  $L^2$  orthonormalized RB, the following estimate holds

$$\text{for } n = 0, \dots, \frac{\Delta t_F}{T}, \|u(t^n)(\mu) - u_{Hh}^{N,n}(\mu)\|_{L^2(\Omega)} \leq \varepsilon'(N) + C'_1(H^2 + \Delta t_G^2) + C'_2(h^2 + \Delta t_F), \quad (34)$$

where  $C'_1$  and  $C'_2$  are constants independent of  $h$ ,  $H$  and  $N$ , and  $\varepsilon'$  depends on the Kolmogorov  $N$ -width, and corresponds to the  $L^2$  error between the fine solution and its projection on the reduced space.

We now go on with the proof of Theorem 4.1.

*Proof.* The NIRB approximation at time step  $n = 0, \dots, \frac{T}{\Delta t_F}$ , for a new parameter  $\mu \in \mathcal{G}$  is defined by (16). Thus, the triangle inequality gives

$$\cancel{\|u(t)(\mu) - u_{Hh}^{N,n}(\mu)\|_{H^1(\Omega)}}, \quad (35)$$

$$\begin{aligned} \|u(t)(\mu) - u_{Hh}^{N,n}(\mu)\|_{H^1(\Omega)} &\leq \|u(t)(\mu) - u_h^n(\mu)\|_{H^1(\Omega)} + \|u_h^n(\mu) - u_{hh}^{N,n}(\mu)\|_{H^1(\Omega)} + \|u_{hh}^{N,n}(\mu) - u_{Hh}^{N,n}(\mu)\|_{H^1(\Omega)} \\ &=: T_1 + T_2 + T_3, \end{aligned} \quad (36)$$

where  $u_{hh}^{N,n}(\mu) = \sum_{i=1}^N (u_h^n(\mu), \Phi_i^h) \Phi_i^h$ .

- The first term  $T_1$  may be estimated using the inequality (21), such that

$$\|u(t)(\mu) - u_h^n(\mu)\|_{H^1(\Omega)} \leq C(\mu) (h + \Delta t_F). \quad (37)$$

- We denote by  $S_h = \{u_h(\mu), \mu \in \mathcal{G}\}$  the set of all the solutions. For our model problem, this manifold has a low complexity. It means that for an accuracy  $\varepsilon = \varepsilon(N)$  related to the Kolmogorov  $N$ -width of the manifold  $S_h$ , for any  $\mu \in \mathcal{G}$ , and any  $n \in 0, \dots, \frac{T}{\Delta t_F}$ ,  $T_2$  is bounded by  $\varepsilon$  which depends on the Kolmogorov  $N$ -width.

$$T_2 = \left\| u_h^n(\mu) - \sum_{i=1}^N (u_h^n(\mu), \Phi_i^h) \Phi_i^h \right\|_{H^1(\Omega)} \leq \varepsilon(N). \quad (38)$$

- The third term  $T_3$  depends on the method used to create the RB.

- Let us first consider the greedy approach with a Gram-Schmidt procedure and an eigenvalue problem (29), which yields to an orthogonalization in  $L^2$  and in  $H_1$ . Therefore,

$$\|u_{hh}^{N,n} - u_{Hh}^{N,n}\|_{H^1(\Omega)}^2 = \sum_{i=1}^N |(u_h^n(\mu) - \tilde{u}_H^n(\mu), \Phi_i^h)|^2 \|\Phi_i^h\|_{H^1(\Omega)}^2, \quad (39)$$

where  $\tilde{u}_H^n(\mu)$  is the quadratic interpolation of the coarse snapshots on time  $t^n \forall n = 0, \dots, \frac{T}{\Delta t_F}$ , defined by (30). Indeed, we want to recover the second order in time of the Crank-Nicolson scheme and a linear reconstruction in time leads to suboptimal bounds [20].

From the RB orthonormalization in  $L_2$ , the equation (29) yields

$$\|\Phi_i^h\|_{H^1}^2 := \|\nabla \Phi_i^h\|_{L^2(\Omega)}^2 = \lambda_i \|\Phi_i^h\|_{L^2(\Omega)}^2 = \lambda_i \leq \max_{i=1, \dots, N} \lambda_i = \lambda_N, \quad (40)$$

such that the equation (39) yields

$$\|u_{hh}^{N,n} - u_{Hh}^{N,n}\|_{H^1(\Omega)}^2 \leq C \lambda_N \|u_h^n(\mu) - \tilde{u}_H^n(\mu)\|_{L^2(\Omega)}^2. \quad (41)$$

Now by definition of  $\tilde{u}_H^n(\mu)$  and by theorem 26, for  $t^n \in I_m$ ,

$$\|u_h^n(\mu) - \tilde{u}_H^n(\mu)\|_{L^2} \leq \|u_h^n(\mu) - \tilde{u}_h(t^n)(\mu)\|_{L^2} + \|u_h(t^n)(\mu) - \tilde{u}_H^n(\mu)\|_{L^2} \leq C(\mu) (H^2 + \Delta t_F^2), \quad \text{since } \Delta t_G^2 \simeq \Delta t_F, \quad (42)$$

and we end up for equation (41) with

$$\|u_{hh}^{N,n} - u_{Hh}^{N,n}\|_{H^1(\Omega)} \leq C \sqrt{\lambda_N} (H^2 + \Delta t_F^2), \quad (43)$$

where  $C$  does not depend on  $N$ . Combining these estimates (37), (38) and (43), we obtain the estimate (33).

2. Now we consider only an  $L^2$ -orthonormalized basis, which we will denote  $(\Psi_{h,i})_{i=1,\dots,N}$  (obtained by a Gram-Schmidt algorithm or with the Greedy-POD algorithm 1). The functions  $(\Psi_{h,i})_{i=1,\dots,N}$  and  $(\Phi_i^h)_{i=1,\dots,N}$  are both generators of  $X_h^N$ . Thus, there exists  $(\gamma^i)_{i=1,\dots,N} \in \mathbb{R}^N$  such that  $\Psi_{h,i} = \sum_{j=1}^N \gamma_j^i \Phi_i^h$ .

By the  $H^1$ -orthogonality of the  $(\Phi_i^h)_{j=1,\dots,N}$ , it follows

$$\begin{aligned} \|\Psi_{h,i}\|_{H^1}^2 &= \sum_{j=1}^N |\gamma_j^i|^2 \|\Phi_i^h\|_{H^1}^2, \\ &\leq \lambda_N \sum_{j=1}^N |\gamma_j^i|^2 \|\Phi_i^h\|_{L^2(\Omega)}^2 \text{ by equation (29),} \\ &= \lambda_N \|\Psi_{h,i}\|_{L^2(\Omega)}^2 \text{ by the } L^2\text{-orthogonality of the } (\Psi_{h,i}^n)_{i=1,\dots,N}. \end{aligned} \quad (44)$$

From the estimate (44) and the  $L_2$ -orthonormalization of the RB,

$$\begin{aligned} \|u_{hh}^{N,n}(\mu) - u_{Hh}^{N,n}(\mu)\|_{H^1} &\leq \sum_{i=1}^N |(u_h^n(\mu) - \tilde{u}_H^n(\mu), \Psi_{h,i}^n)| \|\Psi_{h,i}\|_{H^1}, \\ &\leq C \sqrt{\lambda_N} \sum_{i=1}^N |(u_h^n(\mu) - \tilde{u}_H^n(\mu), \Psi_{h,i}^n)|. \end{aligned} \quad (45)$$

From Cauchy-Schwarz inequality, inequality (45) leads to

$$\begin{aligned} \|u_{hh}^{N,n}(\mu) - u_{Hh}^{N,n}(\mu)\|_{H^1} &\leq C \sqrt{\lambda_N} \sqrt{N} \sqrt{\sum_{i=1}^N |(u_h^n(\mu) - \tilde{u}_H^n(\mu), \Psi_{h,i}^n)|^2}, \\ &\leq C \sqrt{\lambda_N} \sqrt{N} \|u_h^n(\mu) - \tilde{u}_H^n(\mu)\|_{L^2(\Omega)}, \end{aligned}$$

and we end up with

$$\|u_{hh}^{N,n}(\mu) - u_{Hh}^{N,n}(\mu)\|_{H^1} \leq C \sqrt{N} \sqrt{\lambda_N} (h^2 + \Delta t_G^2), \quad (46)$$

which leads to estimate (33) using the inequalities (37), (38), and (46), and concludes the proof.  $\square$

150 **Remark 4.4.** Note that, from the proof of Theorem 4.1, the estimate of the method implemented with an only  $L^2$  orthonormalized basis set has an additional  $\sqrt{N}$  factor (where  $N$  is the number of modes) compared to the one obtained from the  $L^2$  and  $H^1$  orthogonalized basis set. Thus, the NIRB approximation is stabilized with the  $H^1$  orthogonality, compared with a RB only orthogonalized in  $L^2$ . This difference may be numerically observed on more complex numerical results which require more modes [11].

155  **$L^2$  estimate.** We proceed with the proof of theorem 4.3.

*Proof.* In analogy with the  $H^1$  estimate, we have

$$\begin{aligned} \forall n = 0, \dots, \frac{T}{\Delta t_F}, \|u(t^n)(\mu) - u_{Hh}^{N,n}(\mu)\|_{L^2} &\leq \|u(t^n)(\mu) - u_h^n(\mu)\|_{L^2} + \|u_h^n(\mu) - u_{hh}^{N,n}(\mu)\|_{L^2} + \|u_{hh}^{N,n}(\mu) - u_{Hh}^{N,n}(\mu)\|_{L^2} \\ &=: T_1 + T_2 + T_3. \end{aligned} \quad (47)$$

- For the first term  $T_1$ , it follows theorem 2.4 that

$$T_1 \leq C(h^2 + \Delta t_F). \quad (48)$$

- As with the  $H^1$  estimate,  $T_2$  can be estimated with the Kolmogorov N-width, and thus, for an accuracy  $\varepsilon' = \varepsilon'(N) \leq \varepsilon(N)$ ,

$$T_2 \leq \varepsilon'. \quad (49)$$

*On note un  $\Sigma'$  à la place de  $\Sigma$   
parce que tu mesures en norme  $L^2$ ,  
si c'est cela il faut l'expliquer*

- For the last term  $T_3$ , by  $L^2$ -orthonormality,

$$\begin{aligned} \|u_{hh}^{N,n}(\mu) - u_{Hh}^{N,n}(\mu)\|_{L^2(\Omega)}^2 &= \sum_{i=1}^N |(u_h^n(\mu) - u_H^n(\mu), \Psi_{h,i}^n)|^2 \|\Phi_i^h\|_{L^2(\Omega)}^2, \\ &\leq C \|u_h^n(\mu) - u_H^n(\mu)\|_{L^2(\Omega)}. \end{aligned} \quad (50)$$

By theorem 26 and triangle inequality, it leads to

$$\|u_{hh}^{N,n}(\mu) - u_{Hh}^{N,n}(\mu)\|_{L^2(\Omega)}^2 \leq C (H^2 + \Delta t_G^2). \quad (51)$$

Combining (47) with (48), (49), (51) concludes the proof. □

## 5 Numerical results.

In this section, we applied the NIRB algorithm on several numerical tests and in each case, we compared NIRB errors without the rectification post-treatment with rectified NIRB errors 3:

- First, on the model problem (8) with  $\Delta t_G \simeq H \simeq \frac{h}{2} \simeq \frac{\Delta t_F}{2}$ . Note that in some situations, because of the constants  $C_2$  and  $C_4$  in the estimate of theorem 4.1, the best size for the coarse mesh may not be  $\Delta t_F^{1/2}$ . We observe that the NIRB with and without the rectification gives the same accuracy as with the fine solutions.
- Then, on the model problem with  $\Delta t_G^2 \simeq H \simeq \sqrt{h} \simeq \Delta t_F$ . The error with the NIRB method is reduced compared to the coarse FEM errors, and with the rectification post-treatment, we retrieve the fine FEM errors. We retrieved the rates of convergence expected from theorem 4.1 in  $\mathcal{O}(h + \Delta t_F)$  for both with and without the rectification post-processing algorithm.
- Finally, we also tested our problem on a more complex problem, which is the Brusselator equations, and retrieve the fine accuracy with the NIRB and the rectification postprocessing algorithms.

We implemented both schemes on FreeFem ++ (version 4.9) [15] in order to retrieve the fine and coarse snapshots, and save the solutions in VTK format. Then we applied the NIRB/ NIRB rectified algorithm with python, in order to highlight the non-intrusive side of this method (as in [11]). After saving the NIRB approximations with Paraview module on Python, the errors have been computed with FreeFem++.

### 5.1 $\Delta t_G \simeq H \simeq \frac{h}{2} \simeq \frac{\Delta t_F}{2}$ .

We took  $\mathcal{G} = (0, 10)$  and as our right-hand side function

$$f(t, \mathbf{x}) = 10[x^2(x-1)^2y^2(y-1)^2 - 2t((6x^2 - 6x + 1)(y^2(y-1)^2) + (6y^2 - 6y + 1)(x^2(x-1)^2))], \quad (52)$$

where  $\mathbf{x} = (x, y)$ .

We took 19 parameters in  $\mathcal{G}$  for the RB construction such that  $\mu_i = 0.5i$ ,  $i = 1, \dots, 19$  and  $t_0 = 1$ , and  $T = 2$  (note that the coarse time grid must belong to the interval of the fine one). We tried our algorithms on several size of meshes, always with  $\Delta t_F \simeq h$  and  $\Delta t_G \simeq H$  (both schemes are stables).

Figure 1 presents the results of the NIRB algorithm (with POD-Greedy) for a new parameter  $\mu = 1$  (so we removed this parameter for the construction of the snapshots). We plotted the  $H_0^1$  errors both with and without the rectification post-treatment, and these errors are compared to the fine and coarse FEM errors. The exact solution is given by

$$u(t, \mathbf{x}; 1) = 10tx^2(1-x)^2y^2(1-y)^2.$$

The rectification post-processing step is done for each time step. Thus the NIRB with rectification is given by

$$Ru_{Hh}^{N,n}(\mu) = \sum_{i,j=1}^N R_{ij}^n \alpha_j^H(\mu, t^n) \Phi_i^h(\mathbf{x}), \quad n \geq 0, \quad (53)$$

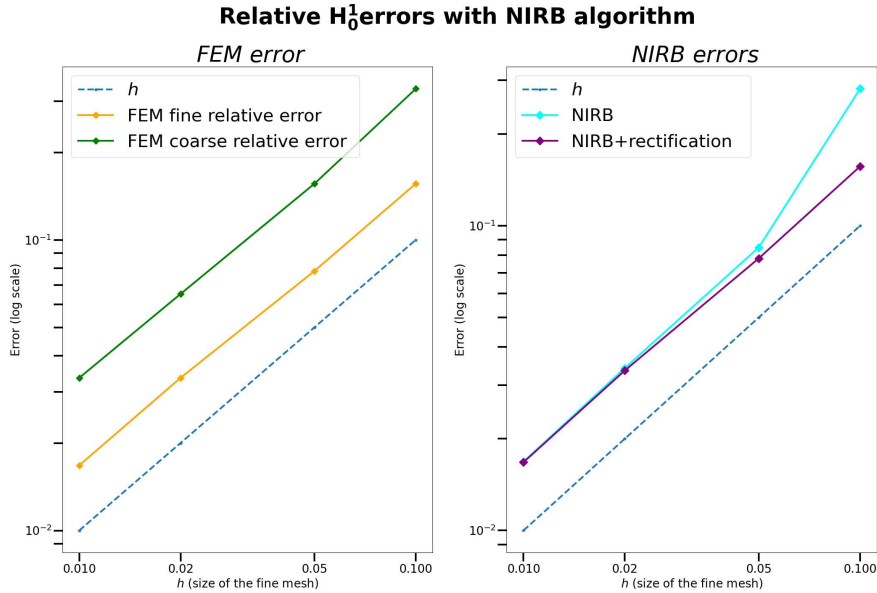


Figure 1:  $\Delta t_G \simeq H \simeq \frac{h}{2} \simeq \frac{\Delta t_F}{2}$ . Convergence rate for  $\mu = 1$  (as a new parameter): FEM  $H_0^1$  relative errors (56) for several sizes of mesh (left) compared to the NIRB method with ( $N = 3$ ) and without the rectification post-treatment ( $N = 3$ ) (55)

180 where the rectification matrix  $R$  may be seen as an indexed (by  $n$ ) family of 2nd-order tensor.

The relative errors are computed in the maximum-norm in time. The  $H_0^1$  NIRB error is defined as

$$\frac{\|u(\mu) - u_{Hh}^N(\mu)\|_{L^\infty(t_0, T; H_0^1(\Omega))}}{\|u(\mu)\|_{L^\infty(t_0, T; H_0^1(\Omega))}}, \quad (54)$$

and with the rectification post-treatment we have

$$\frac{\|u(\mu) - Ru_{Hh}^N(\mu)\|_{L^\infty(t_0, T; H_0^1(\Omega))}}{\|u(\mu)\|_{L^\infty(t_0, T; H_0^1(\Omega))}}, \quad (55)$$

where  $Ru_{Hh}^N$  is defined by (53), and these relative errors are compared to the FEM ones defined as

$$\frac{\|u(\mu) - u_h(\mu)\|_{L^\infty(t_0, T; H_0^1(\Omega))}}{\|u(\mu)\|_{L^\infty(t_0, T; H_0^1(\Omega))}} \text{ and } \frac{\|u(\mu) - u_H(\mu)\|_{L^\infty(t_0, T; H_0^1(\Omega))}}{\|u(\mu)\|_{L^\infty(t_0, T; H_0^1(\Omega))}}. \quad (56)$$

We also plotted the  $L^2$  errors in Figure 2. We can see that the NIRB  $L^2$  relative error without rectification is very close to the coarse  $L^2$  relative error, thus, in the  $L^2$  norm, no amelioration is provided by the NIRB algorithm, however with the rectification post-treatment, the error reaches the fine accuracy.

Finally, in order to evaluate the NIRB algorithm with respect to the parameters, table 1 presents the maximum  $H_0^1$ -error of the NIRB rectified approximation over the parameters. The error is given by

$$\max_{\mu \in \mathcal{G}_{Ntrain}} \frac{\|u_h(\mu) - Ru_{Hh}^N(\mu)\|_{L^\infty(t_0, T; H_0^1(\Omega))}}{\|u_h(\mu)\|_{L^\infty(t_0, T; H_0^1(\Omega))}}. \quad (57)$$

and the maximum in our training parameters is retrieved for  $\mu = 9$ .

### 5.1.1 Time execution (min,sec)

We present the FEM and NIRB runtimes in 2 and 3.

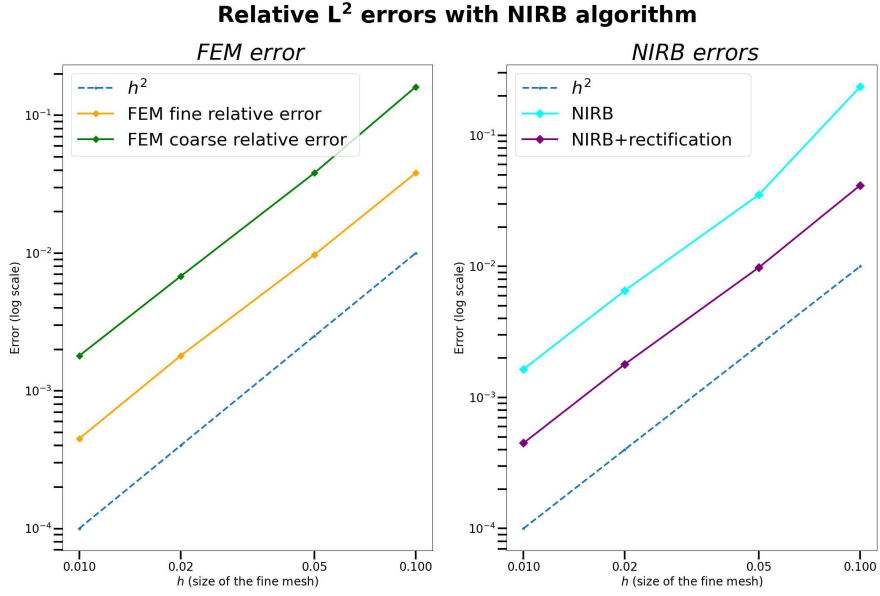


Figure 2:  $\Delta t_G \simeq H \simeq \frac{h}{2} \simeq \frac{\Delta t_F}{2}$ . Convergence rate for  $\mu = 1$  (as a new parameter): FEM  $L^2$  relative errors for several sizes of mesh (left) compared to NIRB with ( $N = 3$ ) and without the rectification post-treatment ( $N = 3$ ) (right)

Table 1: Maximum  $H_0^1$  error over the parameters [ $\mu = 9$ ] (57) (compared to the true NIRB projection and to the FEM coarse projection) with  $N = 20$  with  $h = 0.01$

NIRB rectified error	$\max_{\mu \in \mathcal{G}_{Ntrain}} \frac{\ u_h(\mu) - u_{hh}^N(\mu)\ _{L^\infty(t_0, T; H_0^1(\Omega))}}{\ u_h(\mu)\ _{L^\infty(t_0, T; H_0^1(\Omega))}}$	$\max_{\mu \in \mathcal{G}_{Ntrain}} \frac{\ u_h(\mu) - u_H(\mu)\ _{L^\infty(t_0, T; H_0^1(\Omega))}}{\ u_h(\mu)\ _{L^\infty(t_0, T; H_0^1(\Omega))}}$
$4.84 \times 10^{-5}$	$2.31 \times 10^{-10}$	$1.42 \times 10^{-1}$

Table 2: FEM runtimes

FEM high fidelity solver	FEM coarse solution
00:	00:02

Table 3: NIRB runtimes ( $N = 10$ )

NIRB Offline	classical rectified NIRB online
1:45	00:02

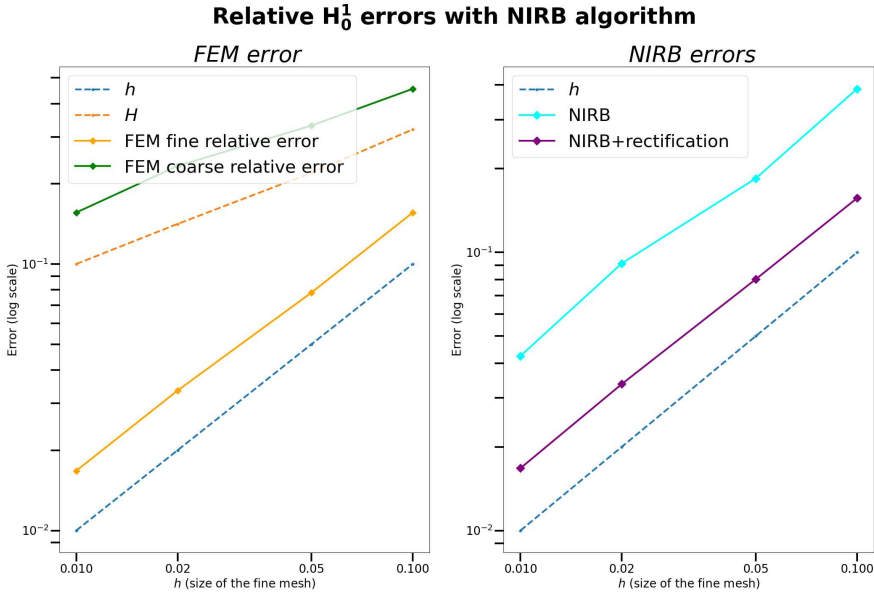


Figure 3:  $H^2 \simeq h \simeq \Delta t_G^2 \simeq \Delta t_F$ , Convergence rate for  $\mu = 1$  (as a new parameter): FEM relative  $H_0^1$  errors for several sizes of mesh (left) compared to NIRB with ( $N=3$ ) and without the rectification post-treatment ( $N = 3$ ) (right)

## 5.2 $H^2 \simeq h \simeq \Delta t_G^2 \simeq \Delta t_F$

As previously, in Figure 3 we display the convergence rate of the fine approximations (left) and of the NIRB approximations (with and without rectification). For all meshes, we choose  $\mu = 1$  and as expected, we observe that both NIRB errors converge in  $\mathcal{O}(h + \Delta t_F)$ , and we retrieved the fine accuracy with the rectified approximation.

We also plotted the  $L^2$  errors in Figure 4.

Finally, in order to evaluate the NIRB algorithm with respect to the parameters, table 4 presents the maximum  $H_0^1$ -error of the NIRB rectified approximation over the parameters. The error is given by (57), and the maximum in our training parameters is retrieved for  $\mu = 9$ .

Table 4: Maximum  $H_0^1$  error over the parameters [ $\mu = 9$ ] (57) (compared to the true NIRB projection and to the FEM coarse projection) with  $N = 20$  with  $h = 0.01$

NIRB rectified error	$\max_{\mu \in \mathcal{G}_{Ntrain}} \frac{\ u_h(\mu) - u_{hh}^N(\mu)\ _{L^\infty(t_0, T; H_0^1(\Omega))}}{\ u_h(\mu)\ _{L^\infty(t_0, T; H_0^1(\Omega))}}$	$\max_{\mu \in \mathcal{G}_{Ntrain}} \frac{\ u_h(\mu) - u_H(\mu)\ _{L^\infty(t_0, T; H_0^1(\Omega))}}{\ u_h(\mu)\ _{L^\infty(t_0, T; H_0^1(\Omega))}}$
$4.21 \times 10^{-3}$	$1.40 \times 10^{-9}$	$7.80 \times 10^{-1}$

### 5.2.1 Time execution (min,sec)

We present the FEM and NIRB runtimes in 5 and 6.

Table 5: FEM runtimes

FEM high fidelity solver	FEM coarse solution
00:03	00:01

We observe that the errors without the rectification post-treatment increases with  $N$  due to the role of the constants  $C_2$  and  $C_4$  in the estimate of theorem 4.1, whereas with the post-treatment they remain stable. This is illustrated by Figure Figure 5 where the  $H_0^1$  errors are displayed for  $\mu = 1$  and different number of modes  $N$ .

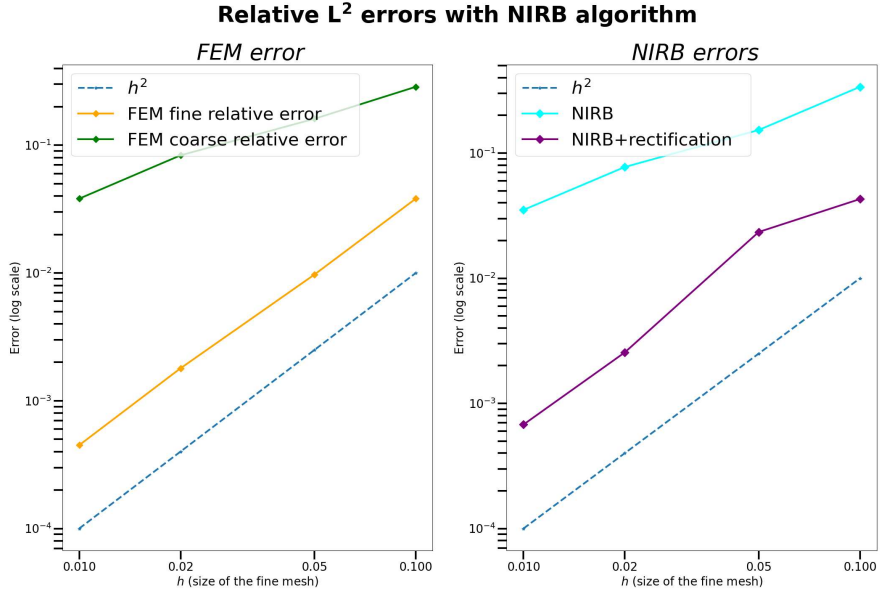


Figure 4:  $H^2 \simeq h \simeq \Delta t_G^2 \simeq \Delta t_F$ , Convergence rate for  $\mu = 1$  (as a new parameter): FEM  $L^2$  relative errors for several sizes of mesh (left) compared to NIRB with ( $N = 3$ ) and without the rectification post-treatment ( $N = 3$ ) (right)

Table 6: NIRB runtimes ( $N = 10$ )

NIRB Offline	classical rectified NIRB online
1:32	00:02

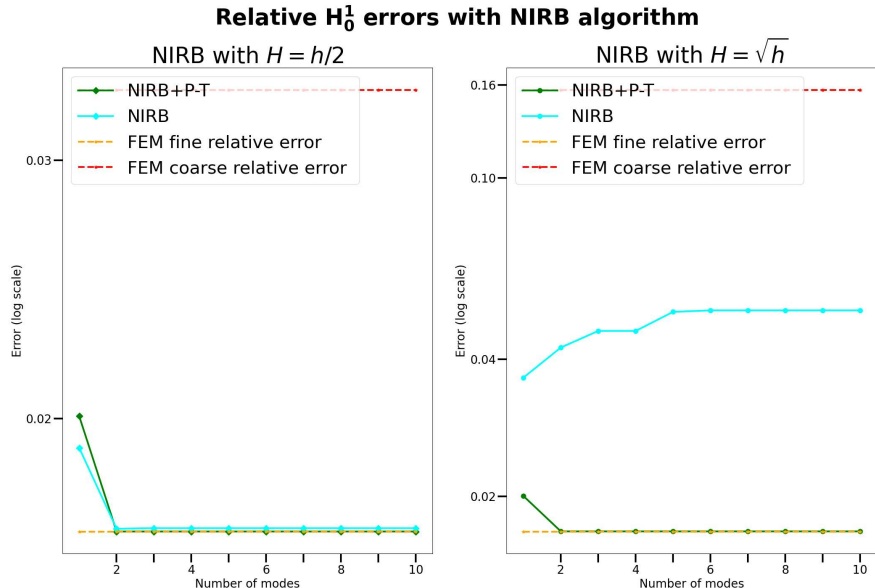


Figure 5: For  $h = 0.01$ :  $H = \frac{h}{2}$  (left),  $H = h^2$  (right),  $\mu = 1$ , NIRB relative  $H_0^1$  errors and rectified NIRB (+ P-T)  $H_0^1$  compared to FEM errors with different modes  $N$

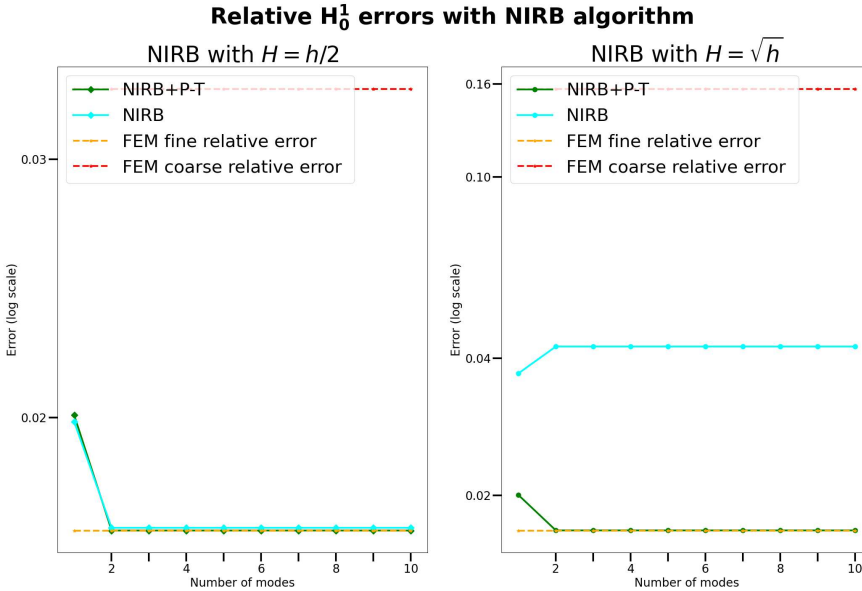


Figure 6: For  $h = 0.01$ :  $H = 2h$  (left),  $H = h^2$  (right),  $\mu = 1$ , NIRB relative  $H_0^1$  errors and rectified NIRB (+ P-T)  $H_0^1$  compared to FEM errors with different modes  $N$  using the other NIRB decomposition (58)

**Remark 5.1.** We may also consider NIRB approximations of (14) under the form

$$u_{Hh}^{N,n}(\mathbf{x}; \mu) = \sum_{i=1}^N \alpha_i^H(\mu, t^n) \Phi_{h,i}^n(\mathbf{x}), \quad n \geq 0, \quad (58)$$

with  $(\Phi_{h,i}^n)_{i=1,\dots,N}$  time-dependent basis functions. This time, the greedy algorithm 2 is executed for each time step and thus, this method is less efficient (in term of storage) since we have to store  $N$  times the number of time steps of the reduced basis.

With this decomposition, we obtained the following results (see Figure 6).

### 205 5.3 Brusselator equations

We consider a last test more complex, involving chemical reactions, which is the Brusselator problem [21]. For this problem, the chemical concentrations are controlled by parameters throughout the reaction process, which makes it interesting as an application of our NIRB method. Indeed, this problem may be seen as an optimization problem over the parameters. Thus, let us consider the Brusselator problem in a spatial domain  $\Omega = [0, 1]^2$  and with an ending time  $T = 5$ . The two-dimensional reaction-diffusion Brusselator system is the non-linear system of partial differential equations (with Neumann boundary conditions)

$$\begin{cases} \partial_t u_1 = a + u_1 u_2^2 - (b + 1)u_1 + \alpha \Delta u_1, & \text{in } \Omega \times ]0, T] \\ \partial_t u_2 = bu_1 - u_1 u_2^2 + \alpha \Delta u_2, & \text{in } \Omega \times ]0, T], \\ u_1(\mathbf{x}, 0) = u_0(\mathbf{x}) = 2 + 0.25y, & \text{in } \Omega \\ u_2(\mathbf{x}, 0) = v_0(\mathbf{x}) = 1 + 0.8x, & \text{in } \Omega, \\ \partial_n u_1 = 0, & \partial\Omega, \\ \partial_n u_2 = 0, & \partial\Omega. \end{cases}$$

Now, we have to deal with a non-linearity, and two unknowns. Our parameter belongs to  $\mathbb{R}^3$ ,  $\mu = (a, b, \alpha)$ .  
 215 For the implementations, we use an Euler implicit scheme for the fine solutions with the Newton algorithm to deal with the non-linearity and an explicit 2nd order Runge-Kutta scheme (RK2) for the coarse mesh (thus the coarse approximation is computed much faster). Indeed, with an explicit Euler scheme, the solution blows up whereas for a scheme of order 2 (as RK2) it is stable for our parameters.

We tested our NIRB algorithm on stable solutions ( $b \leq 1 + a^2$ ). For  $\alpha$  small enough, the solutions  $(u_1, u_2)$  converge to  $(u_l, v_l) = (a, \frac{b}{a})$ , which may be verified by our NIRB approximation below as presented in Figure 8,

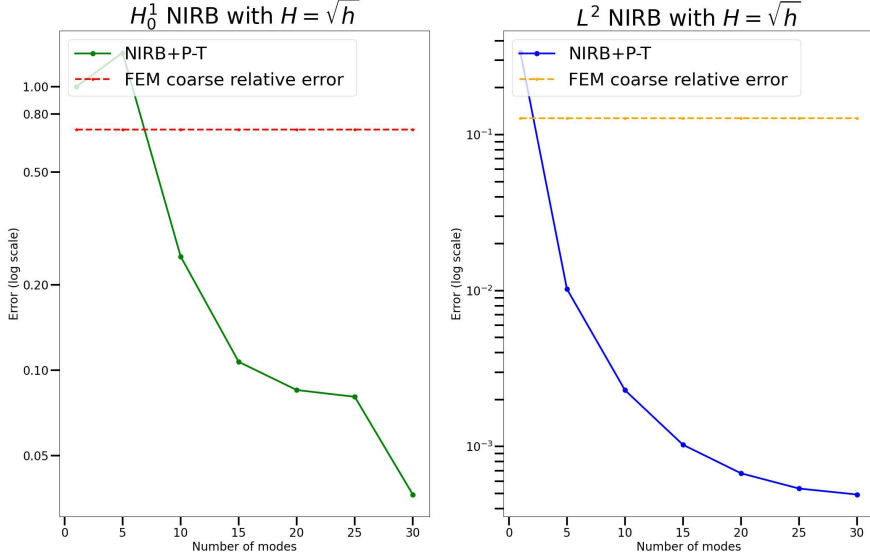


Figure 7: Test with  $L^\infty(0, T; H^1(\Omega))$  relative errors with a new parameter  $(a, b, \alpha) = (3, 2, 0.008)$ ,  $t_0 = 0$ ,  $T = 5$ ,  $\Omega = [0, 1] \times [0, 1]$  (NIRB+ rectification post-treatment compared to coarse FEM error)

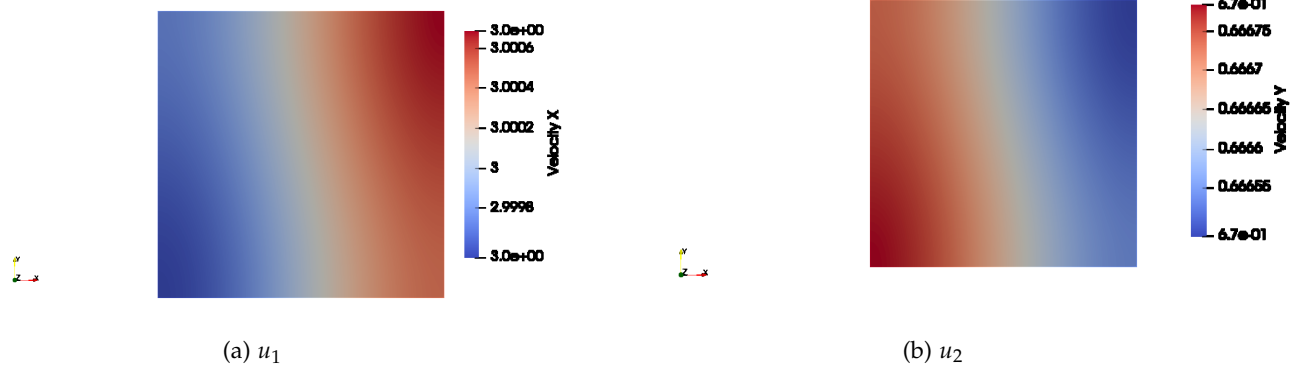


Figure 8: NIRB approximations ( $u_1$  (left) and  $u_2$  (right)) for  $T = 5$  with  $N = 10$  modes (close to  $(a, \frac{b}{a}) = (3, 2/3)$ )

thus we choose several snapshots with the parameters  $(a, b, \alpha) \in [2, 4] \times [1, 4] \times [0.001, 0.05]$ , and more precisely we took  $a = 2, 2.5, 4$ ,  $b = 1, 3, 4$  and  $\alpha = 0.001, 0.005, 0.01, 0.05$ , and tested our algorithm on the new parameter  $(a, b, \alpha) = (3, 2, 0.008)$  with  $h = 0.02 = \Delta t_F \simeq H^2 = \Delta t_G^2$  ( $\Delta T_G = H = 0.1$ ). The relative  $H_0^1$  errors of the NIRB approximation with rectification post-treatment (55) and of the FEM fine approximation (56) are displayed in Figure 7. Here, we do not know the exact solution but we observe a gain of accuracy of factor 10 with 25 modes on the relative  $H_0^1$  error with the NIRB solution compared to the coarse FEM one (with 30 modes, the error drops to  $3.64 \times 10^{-2}$ , compared to  $7.06 \times 10^{-1}$  with the FEM approximation).

In Figure 8 follows the NIRB rectified solution for  $N = 10$  modes at time  $T = 5$  for the two variables  $u_1$  and  $u_2$ . The approximation is close to  $(a, \frac{b}{a}) = (3, 2/3)$  as expected.

Finally, the computational costs are well saved during the online part of the algorithm as it is highlighted with this example. Indeed, since there is a non-linearity, the system must be solved several times for each time step, and thus is quite expensive for a high-fidelity approximation.

### 5.3.1 Time execution (min,sec)

We present the FEM and NIRB runtimes in 7 and 8.

Table 7: FEM runtimes (min:sec)

FEM high fidelity solver	FEM coarse solution
4:52	00:02

Table 8: NIRB runtimes ( $N = 10$ , h:min:sec)

NIRB Offline	classical rectified NIRB online
1:53:00	00:04:00

235

## 6 Estimates on the rectification

As observed in our numerical results, the rectification post-treatment allows us to retrieve the error of the fine solutions. This section aims to understand how it works and takes its inspiration from a previous work [19]. We refer to chapter 7 of [19] for the notations.

240 In the elliptic context, the rectification matrix is defined by (3), whereas in the parabolic context, it is given by algorithm 3, where a loop in time takes place. Thus, for each time step, the rectification post-treatment works as in the elliptic framework, hence we will stick to the unique notation without the time indices.

In both cases, we deal with three linear operators:

- $\pi_N : V_h \rightarrow X_h^N$ , which represents our fine solutions.
- 245 •  $\mathcal{I}_N : V_H \subset V_h \rightarrow X_h^N$ , which is our coarse solutions.
- $\tilde{\pi}_N : V_H \subset V_h \rightarrow X_h^N$ , which is our rectification operator, which goes from coarse to fine coefficients.

Notation:

$u_{hh}^N$ : true approximation,  $u_{Hh}^N$ : NIRB approximation,  $Ru_{Hh}^N$  : Rectified NIRB approximation.

By definition,

$$Ru_{Hh}^N(\mu_k) = u_{hh}^N(\mu_k), \forall k = 1, \dots, N. \quad (59)$$

For  $k = 1, \dots, N$ ,

$$\begin{aligned} \left\| \sum_{i=1}^N (u_h(\mu), \Phi_i^h) \Phi_i^h - \sum_{i,j=1}^N R_{i,j}(u_H(\mu), \Phi_j^h) \Phi_i^h \right\|_{H^1(\Omega)} &\leq \left\| \sum_{i=1}^N (u_h(\mu) - u_h(\mu_k), \Phi_i^h) \Phi_i^h - \sum_{i,j=1}^N R_{i,j}(u_H(\mu) - u_H(\mu_k), \Phi_j^h) \Phi_i^h \right\|_{H^1(\Omega)}, \\ &\leq \sqrt{\lambda_N} \|u_h(\mu) - u_h(\mu_k)\|_{L^2(\Omega)} + \left\| \sum_{i,j=1}^N R_{i,j}(u_H(\mu) - u_H(\mu_k), \Phi_j^h) \Phi_i^h \right\|_{H^1(\Omega)}, \\ &\leq \sqrt{\lambda_N} \|u_h(\mu) - u_h(\mu_k)\|_{L^2(\Omega)} + \|\tilde{\pi}_N\|_2 \|u_H(\mu) - u_H(\mu_k)\|_{L^2}. \end{aligned}$$

Since the Kolmogorov width is small,

$$E(\mathcal{M}_h, X_h^N) = \sup_{x \in \mathcal{M}_h} (\inf_{y \in X_h^N} \|x - y\|) \quad (60)$$

is small and thus,

$$\inf \|u_h(\mu) - \Phi_h(\mu_k)\| \leq E(\mathcal{M}_h, X_h^N) \quad (61)$$

250 is small too. Now,  $\|u_H(\mu) - u_H(\mu_k)\|_{L^2}$  must be small, so the Kolmogorov width of the coarse solutions needs to be relatively small too. We may numerically prove in our problem model that  $\|\tilde{\pi}_N\|_2$  is in  $\mathcal{O}(1)$ .

## References

- [1] M. Barrault, C. Nguyen, A. Patera, and Y. Maday. An ‘empirical interpolation’ method: application to efficient reduced-basis discretization of partial differential equations. *Comptes rendus de l’Académie des sciences. Série I, Mathématique*, 339-9:667–672, 2004.
- [2] G. Berkooz, P. Holmes, and J L Lumley. The proper orthogonal decomposition in the analysis of turbulent flows. *Annual review of fluid mechanics*, 25(1):539–575, 1993.
- [3] S. Brenner and R. Scott. *The mathematical theory of finite element methods*, volume 15. Springer Science & Business Media, 2007.
- [4] A. Buffa, Y. Maday, A. T. Patera, C. Prud’homme, and G. Turinici. A priori convergence of the greedy algorithm for the parametrized reduced basis method. *ESAIM: Mathematical Modelling and Numerical Analysis-Modélisation Mathématique et Analyse Numérique*, 46(3):595 – 603, 2012.
- [5] F. Casenave, A. Ern, and T. Lelièvre. A nonintrusive reduced basis method applied to aeroacoustic simulations. *Advances in Computational Mathematics*, 41(5):961–986, Jun 2014.
- [6] R. Chakir. *Contribution à l’analyse numérique de quelques problèmes en chimie quantique et mécanique*. PhD thesis, 2009. Doctoral dissertation, Université Pierre et Marie Curie-Paris VI.
- [7] R. Chakir and Y. Maday. A two-grid finite-element/reduced basis scheme for the approximation of the solution of parametric dependent p.d.e. In *9e Colloque national en calcul des structures*, 2009.
- [8] R. Chakir, Y. Maday, and P. Parnaudeau. A non-intrusive reduced basis approach for parametrized heat transfer problems. *Journal of Computational Physics*, 376:pp.617–633, January 2019.
- [9] R. Chakir, B. Streichenberger, and P. Chatellier. A non-intrusive reduced basis method for urban flows simulation. 01 2021.
- [10] L. C. Evans. *Partial differential equations*. American Mathematical Society, Providence, R.I., 2010.
- [11] E. Grosjean. *Variations and further developments on the Non-Intrusive Reduced Basis two-grid method*. PhD thesis, 2022. Thèse de doctorat dirigée par Maday, Yvon Mathématiques appliquées Sorbonne université 2022.
- [12] E. Grosjean and Y. Maday. Error estimate of the non-intrusive reduced basis method with finite volume schemes. *ESAIM: M2AN*, 55(5):1941–1961, 2021.
- [13] B. Haasdonk. Convergence rates of the pod–greedy method. *ESAIM: Mathematical modelling and numerical Analysis*, 47(3):859–873, 2013.
- [14] B. Haasdonk and M. Ohlberger. Reduced basis method for finite volume approximations of parametrized linear evolution equations. *ESAIM: Mathematical Modelling and Numerical Analysis-Modélisation Mathématique et Analyse Numérique*, 42(2):277–302, 2008.
- [15] F. Hecht. New development in freefem++. *Journal of numerical mathematics*, 20(3-4):251–266, 2012.
- [16] J. S. Hesthaven, G. Rozza, and B. Stamm. *Certified reduced basis methods for parametrized partial differential equations*. Springer, 2016.
- [17] D J. Knezevic and A T. Patera. A certified reduced basis method for the fokker–planck equation of dilute polymeric fluids: Fene dumbbells in extensional flow. *SIAM Journal on Scientific Computing*, 32(2):793–817, 2010.
- [18] A. Kolmogoroff. Über die beste annaherung von funktionen einer gegebenen funktionenklasse. *Annals of Mathematics*, pages 107–110, 1936.
- [19] Y. Maday and O. Mula. A generalized empirical interpolation method: application of reduced basis techniques to data assimilation. In *Analysis and numerics of partial differential equations*, pages 221–235. Springer, 2013.
- [20] C. Makridakis. Space and time reconstructions in a posteriori analysis of evolution problems. In *ESAIM: Proceedings*, volume 21, pages 31–44. EDP Sciences, 2007.

- [21] R.C. Mittal and R. Jiwari. Numerical solution of two-dimensional reaction–diffusion brusselator system. *Applied Mathematics and Computation*, 217(12):5404–5415, 2011.
- [22] A. Quarteroni, A. Manzoni, and F. Negri. *Reduced Basis Methods for Partial Differential Equations: an introduction*, volume 92. Springer, 2015.
- [23] B. Streichenberger. *Approches multi-fidélités pour la simulation rapide d’écoulements d’air en milieu urbain*. PhD thesis, 2021. Thèse de doctorat, Université Gustave Eiffel.
- [24] V. Thomée. *Galerkin finite element methods for parabolic problems*, volume 25. Springer Science & Business Media, 2007.